

# High depth of field microscopic imaging using an interferometric camera

P. Potuluri, M. R. Fetterman and D. J. Brady

*Beckman Institute, University of Illinois at Urbana-Champaign,  
Urbana, IL 61801*

*dbrady@duke.edu*

**Abstract:** We describe the design of a microscope combining rotational shear interferometer (RSI)-based coherence imaging with an objective lens to simultaneously obtain high numerical aperture and high depth of field imaging. We present experimental results showing the operation of this instrument.

© 2001 Optical Society of America

OCIS codes: (180.0180) Microscopy; (110.1650) Coherence imaging

---

## References and links

1. Daniel L. Marks, Ronald A. Stack, David J. Brady, David C. Munson and Rachael B. Brady, "Visible Cone-Beam tomography with a lensless interferometric camera," *Science* **284**, 2164-2166 (1999).
2. Daniel L. Marks, Ronald A. Stack and David J. Brady "Three-dimensional coherence imaging in the Fresnel domain" *Appl. Opt.* **8**, 1332-1342 (1999).
3. Sara Bradburn, Thomas W. Cathey and Edward R. Dowski, Jr. "Realizations of focus invariance in optical-digital systems with wave-front coding" *Appl. Opt.* **35**, 9157-9166 (1997).
4. Sara C. Tucker, Thomas W. Cathey and Edward R. Dowski, Jr. "Extended depth of field and aberration control for inexpensive digital microscope systems," *Opt. Express* **11**, 467-474 (1999), <http://www.opticsexpress.org/oearchive/source/9522.htm>.
5. L. Mandel and E. Wolf, *Optical Coherence and Quantum Optics*, (Cambridge University Press, Cambridge, UK, 1995).
6. J. D. Armitage and A. Lohmann, "Rotary shearing interferometry," *Opt. Acta* **12**, 185-192 (1965).
7. F. Roddier, "Interferometric imaging in optical astronomy," *Phys. Rep.* **170**, 97-166 (1988).
8. K. Itoh and Y. Ohtsuka, "Fourier-transform spectral imaging: retrieval of source information from three-dimensional spatial coherence," *J. Opt. Soc. Am. A* **3**, 94-100 (1986).
9. K. Itoh, T. Inoue, and Y. Ichioka, "Interferometric spectral imaging and optical three-dimensional Fourier transformation," *J.J. Appl. Phys* **29**, L1561-L1564 (1990).
10. Zeiss Microscopes, <http://www.zeiss.com>.
11. E. Hecht, *Optics*, (Addison and Wesley Inc., New York, 1998).

---

## 1 Introduction

In conventional imaging systems there is a trade-off between numerical aperture and depth of field. We have previously discussed the elimination of this trade-off in coherence imaging systems[1, 2]. Coherence systems have an infinite depth of field, but the reconstructed image SNR degrades as a function of the number of independent source channels. One can reduce the effective number of source channels by decreasing the numerical aperture.

Microscopic applications are particularly attractive for coherence imaging because the spatial complexity of microscopic sources is often relatively low while simultaneous demand for high numerical aperture, high resolution and high depth of field is strong. Tomographic reconstruction of microscopic samples in particular requires high depth of field imaging [1].

Researchers have demonstrated various techniques to increase the depth of field of a microscope. One approach is to reduce the aperture of the exit pupil slightly, increasing the depth of field at the expense of low throughput and low resolution.

A more interesting technique is to use a cubic-phase plate, which uses an encoding mask to modulate the  $k_x$  and  $k_y$  components of the field. Then, with appropriate decoding algorithms, an image at the focal plane is recovered with an improved depth of field. However, cubic-phase plate system still has a limited depth of field. The depth of field can be increased by making the cubic-phase plate constant larger. Again, the increased depth of field comes at the price of lower resolution [3, 4].

This paper describes a microscope based on coherence imaging systems, hereafter termed the mRSI, formed by replacing the eyepiece of a light microscope with an RSI (rotational shear interferometer). Just as the purpose of the objective/eyepiece combination in a conventional microscope is to match the numerical aperture of the source to the numerical aperture of the eye, the purpose of the objective/RSI combination in the mRSI is to match the numerical aperture of the source to the numerical aperture of the RSI. The advantage of the RSI over the eye or a camera is that one obtains infinite depth of field in the reconstructed microscopic image without sacrificing numerical aperture.

## 2 mRSI Theory and Design

For a quasi-monochromatic and spatially incoherent source, described by the radiant density  $I_s(r_s)$ , the mutual intensity [5] between two sampling points at  $(\frac{\Delta x}{2}, \frac{\Delta y}{2}, 0)$  and  $(-\frac{\Delta x}{2}, -\frac{\Delta y}{2}, 0)$  under the paraxial approximation is given by [1],

$$J(\Delta x, \Delta y) = \int \frac{I_s(r_s)}{z_s^2} \exp \left[ -j \frac{2\pi}{\lambda z_s} (x_s \Delta x + y_s \Delta y) \right] d^3 r_s \quad (1)$$

Taking an inverse Fourier Transform of Eq. 1 with respect to  $\Delta x$  and  $\Delta y$  we obtain

$$\begin{aligned} S(u, v) &= \int J(\Delta x, \Delta y) \exp [j2\pi(u\Delta x + v\Delta y)] d\Delta x d\Delta y \\ &= \int \frac{I_s(r_s)}{z_s^2} \delta \left( u - \frac{x_s}{\lambda z_s}, v - \frac{y_s}{\lambda z_s} \right) d^3 r_s \end{aligned} \quad (2)$$

It can be seen that  $S(u, v)$  is a line integral of  $\frac{I_s(r_s)}{z_s^2}$  along a ray passing through the points  $(x_s = \lambda z_s u, y_s = \lambda z_s v)$ . If a system can measure the mutual intensity, then Eq. 2 can be used to obtain the source intensity.

We use an RSI [6, 7, 8, 9] to measure the mutual intensity function  $J$ . The RSI, shown schematically in Fig.1, is a Michelson-type interferometer incorporating folding mirrors(prisms) instead of flat reflectors [2]. The primary components are a beam splitter and two folding mirrors. One of the mirrors is mounted on a translation stage to vary the relative optical path  $\Delta z$ . The fold axis of one mirror makes an angle of  $\theta/2$  with respect to x-axis. The fold axis of the other mirror makes an angle of  $-\theta/2$  with respect to x-axis.

If the incident field is  $V(x_f, y_f, z_f)$ , then the field produced on the output arm by reflection from the mirrors is  $V(x_f \cos \theta + y_f \sin \theta, x_f \sin \theta - y_f \cos \theta, z_f + \Delta z)$  and  $V(x_f \cos \theta - y_f \sin \theta, -x_f \sin \theta - y_f \cos \theta, z_f)$ . Thus, the intensity detected at point  $(x_f, y_f)$  on the output arm of the RSI is given by,

$$I(x_f, y_f, x_g, y_g) = I_1 + I_2 + 2\text{Re}\{J(\Delta x, \Delta y, q, \Delta z)\} \quad (3)$$

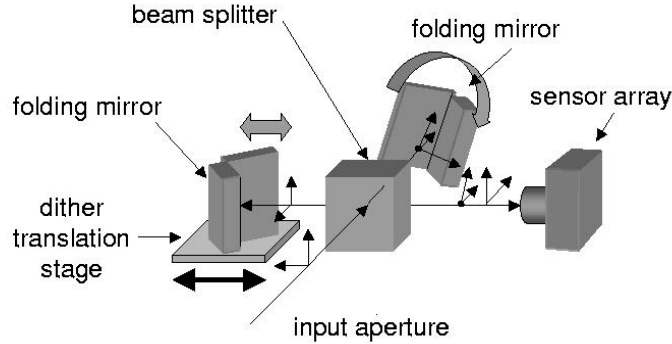


Fig. 1. Schematic diagram of a Rotational Shear Interferometer: RSI is a Michelson interferometer with folding mirrors. The folding axes of the mirrors lie in the transverse plane at angles of  $\theta/2$  and  $-\theta/2$  with respect to the x-axis. The translation stage dithers by a few microns during each image capture.

where

$$\begin{aligned}\Delta x(x_f, y_f) &= 2y_f \sin 2\theta \\ \Delta y(x_f, y_f) &= 2x_f \sin 2\theta \quad \text{and} \\ q(x_f, y_f, x_g, y_g) &= (y_f x_g - x_f y_g) \sin(2\theta)\end{aligned}\quad (4)$$

Here,  $(x_g, y_g)$  is the focal plane center position in global coordinates [2]. Eq. 3 relates the signal measured by the RSI as a function of lateral interferometer position  $(x_g, y_g)$  and the longitudinal scan position to the mutual intensity  $J(\Delta x, \Delta y, q, \Delta z)$ . Once the mutual intensity is known, Eq. 2 can be applied to obtain the object intensity.

Since image reconstruction involves a digital Fourier transformation, the RSI is fundamentally a sampling instrument. The numerical aperture of the RSI is determined by the sampling rate in  $x_f, y_f$  plane and the shear angle  $\theta$ . Assuming a pixel size of  $\Delta$  in the output plane, the numerical aperture of the RSI is

$$N.A. = \frac{\lambda}{\Delta \sin \theta}\quad (5)$$

A typical value of the numerical aperture of the RSI is 0.14 at a shear angle of  $30^\circ$ . Fig. 2 shows a schematic diagram of our optical system. The object is placed under a Zeiss Axioplan transmission-light microscope [10]. As discussed in the previous section, the design goal of the mRSI is to match the numerical aperture of an RSI to the radiant (spatial) bandwidth of the microscopic source. This match is achieved using a high numerical aperture microscope objective. Since the microscope objectives are also designed under paraxial approximations, the approximations used in Eq. 1 are still valid for the mRSI.

Typically microscope objectives are designed to image the source 0.15 m from the objective. However, we are physically constrained as we cannot place the RSI directly at the output of the microscope. In our system configuration, the RSI input aperture is over 0.75m away from the microscope output aperture. Thus, there is a simultaneous requirement for the optical system to match the numerical aperture of the objective with that of the RSI and to redirect the optical field into the RSI input aperture. These requirements can be met by using two intermediate relay lenses of large focal lengths.

The Zeiss objective [10] used in the microscope has a magnification of 10 and a numerical aperture of 0.30. The lens  $L_2$  (focal length  $0.25m$ ) and lens  $L_3$  ( $f = 0.30m$ ) match the numerical aperture of the RSI to that of the objective.

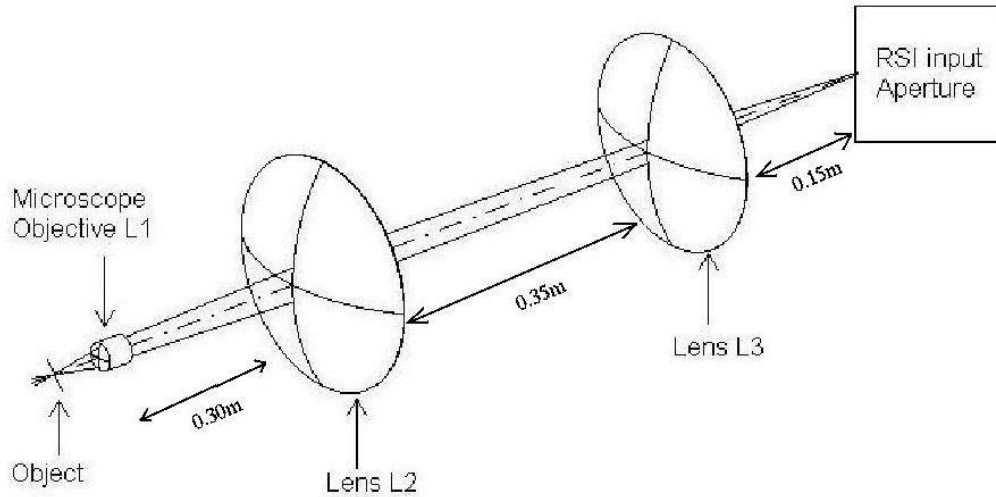


Fig. 2. Schematic diagram of an mRSI

Since mRSI is a combination of the RSI and the microscope objective, the angular resolution of the mRSI will depend on the angular resolution of the RSI and that of the microscope objective. The angular resolution of the microscope objective is given by

$$\Delta\theta = \frac{\text{Aperture diameter}}{0.15 \text{ m}} \quad (6)$$

The aperture diameter of the objective is  $5.7\text{mm}$ . So the angular resolution of the objective is 0.038 radians. The angular resolution of the RSI is given by

$$\Delta\Omega = \frac{\lambda}{N\Delta \sin\theta} \quad (7)$$

where  $N$  is the number of pixels per axis in the RSI sensor plane. We use a red interference filter of bandwidth  $3\text{nm}$  centered at  $\lambda = 0.633\mu\text{m}$  to ensure that the light is quasi-monochromatic. The pixel size of the CCD camera is  $\Delta = 9\mu\text{m}$  and there are 512 pixels per axis on the RSI sensor plane. Note that the angular resolution of the RSI can be varied by adjusting the shear angle  $\theta$ .

Thus, the angular resolution of the mRSI will be limited by the angular resolution of the microscope. The shear angle of the RSI is set such that the angular resolution of the RSI is smaller than that of the objective. For this mRSI, the shear angle is set at  $\theta = 30^\circ$ . At this shear angle, the angular resolution of the RSI is  $2.7 \times 10^{-4} (< 0.038)$  radians.

### 3 Results and Analysis

To demonstrate the high depth of field imaging with the mRSI, we have used a diffraction mask with a spatial frequency of 20 lines/mm. The object has been placed at various distances of (a) 4 mm, (b) 6 mm, (c) 13 mm and (d) 30 mm from the microscope objective.

The object is illuminated with an incoherent white light source, and an interference pattern is formed on the CCD detector array. The dynamic range of the detector is 10 bits. A spectral filter enforces the quasimonochromatic assumption, and the bandwidth of the filter determines the fringe modulation. Large bandwidth filter would decrease

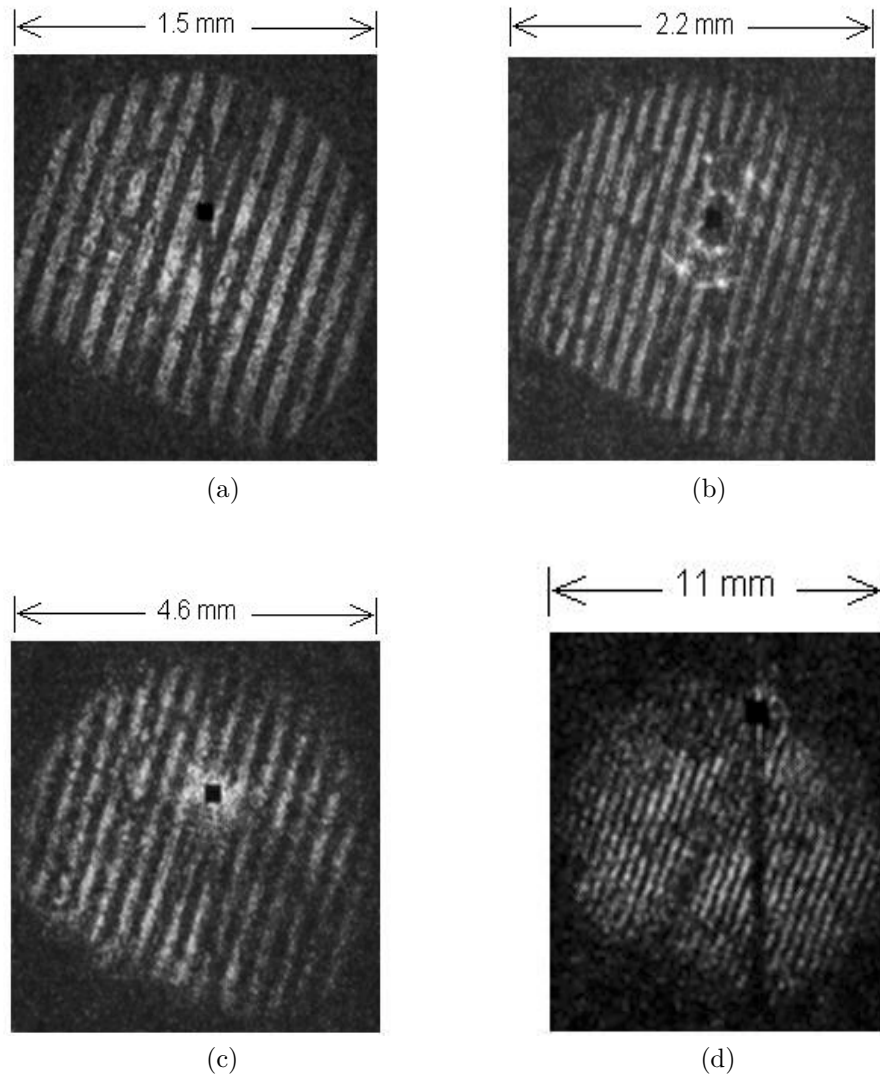


Fig. 3. Images of a diffraction mask obtained from the mRSI: The mask was placed at a distance of (a) 4mm, (b) 6mm, (c) 13mm and (d) 30mm from the objective. The DC component of the Fourier transform has been blocked.

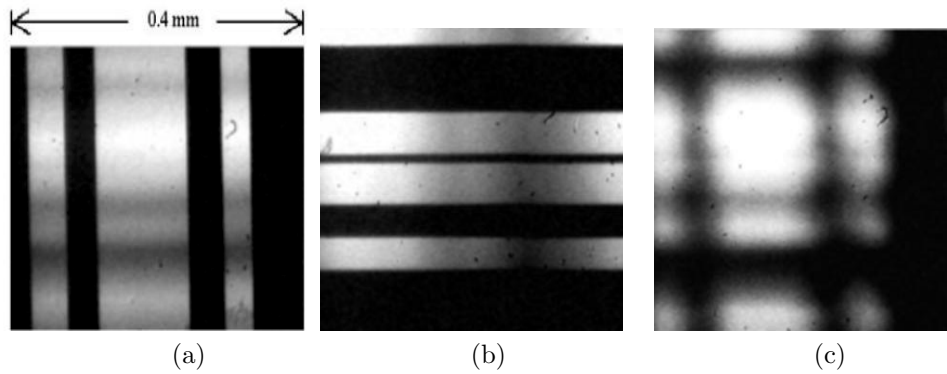


Fig. 4. Images of two combined diffraction masks obtained from a light microscope and video camera

the interference fringe modulation leading to a bad SNR, whereas a very narrow filter will reduce the throughput of the system.

For a quasimonochromatic field, the intensity measured at a point on the RSI sensor plane is

$$I(x_f, y_f) = I_1 + I_2 + 2\text{Re}\{J(\Delta x, \Delta y) \exp(-2\pi il/\lambda)\} \quad (8)$$

The amplitude and phase of the mutual intensity can be isolated by sampling the output plane intensity as a function of optical path difference. For example, if one measures  $I(x_f, y_f)$  for  $l = 0$ ,  $l = \lambda/4$  and  $l = \lambda/2$ , then one can separate  $J(\Delta x, \Delta y)$  from the background intensity.

In practice more than three values of  $l$  are used to reduce the effects of the errors in the translation stage. We choose 16 values of  $l$  ( $l_n = n\lambda/16, n = 0, 1, \dots, 15$ ), and an image is captured corresponding to each delay.  $J(\Delta x, \Delta y)$  can be found using these images and Eq. 8. A discrete Fourier transform of  $J$  will then give the source intensity.

The corresponding images obtained after the digital analysis are shown in Fig. 3. The digital analysis took around 30s for each reconstructed image. Since the detector measures the intensity of the light, which will necessarily be positive, the Fourier transform will always result in a large DC peak at the point (0,0). This point contains no information and hence has been blocked in these images. The angular scale of the image is around  $10^\circ$  and the spatial scale is  $1.5\text{mm}$  for Fig. 3(a). Note that the spatial scales of the images reconstructed depend on the position of the object from the objective.

The working distance of the objective used was  $5.7\text{mm}$ . The depth of field of a conventional microscope is given by [11]  $D = \frac{\lambda}{(N.A.)^2}$ , which is around  $9\mu\text{m}$ . However, it can be clearly seen from the images taken from the mRSI that even if the object is placed around  $3\text{cm}$  away the lens, the image is still in focus. We note that in a conventional microscope, the position of the object from the objective determines the focus of the image and the angular magnification. An advantage of the mRSI is that this distance determines only the angular magnification of the system and not the focus of the final reconstruction.

To further illustrate high depth of field imaging with the mRSI, we have taken two diffraction masks (one containing horizontal lines and the other containing vertical lines) and placed one on top of the other. Fig. 4 shows the images obtained from a camera ( $320 \times 240$  pixels) placed at the output of the microscope. We could focus to either the horizontal lines or to the vertical lines but both lines could not be focussed at a time.

Fig. 5 shows the images of the same masks obtained by the mRSI. It is evident that both the lines are in focus even if an air gap of  $10\text{mm}$  is introduced between them. The spatial scales of the two masks in Fig. 5(b) are different as they are kept at different

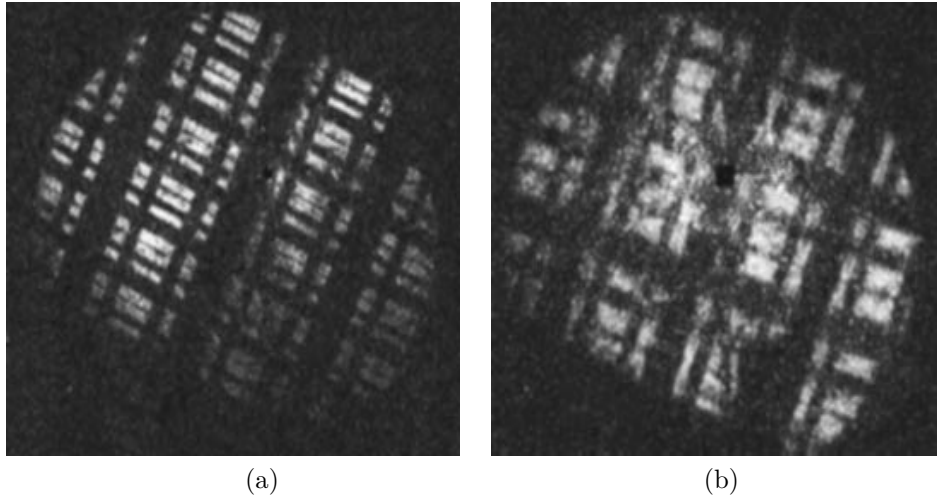


Fig. 5. Images of the two diffraction masks obtained from the mRSI: (a) The masks are placed close to each other, (b) the masks are separated by an air gap of around 10mm. The angular scale of the images is  $10^\circ$ . Note that the two masks have different spatial scales in (b).

distances from the objective.

Thus, high depth of field microscopic images can be obtained with an mRSI. Unfortunately, this very desirable quality comes at a price. In lens-based systems, the signal to noise ratio is proportional to  $\sqrt{N}$ , where  $N$  is the number of photons collected. However, in RSI imaging, the signal-to-noise ratio is proportional to  $\sqrt{N/P}$  where  $P$  is the number of pixels in the RSI image plane [2]. So, the SNR is worse than the standard system by a factor of  $1/\sqrt{P}$ .

#### 4 Conclusion

The mRSI is capable of imaging objects through a microscopic objective with a high depth of field. This should have applications to areas such as biology, fluid mechanics, and material science. In this work, we have shown the design and analysis of the mRSI, along with experimental results. To design the mRSI, it was necessary to calculate the numerical aperture of the RSI and match this with the numerical aperture of the objective lens. Also, we used relay lenses to map the field into the RSI aperture.

For the experimental results in this paper, we studied diffraction masks at various distances from the objective. Comparing this with the images from a camera, we could see that the mRSI results in a high depth of field.

#### 5 Acknowledgements

The authors are grateful to Daniel Marks, Jason Gallicchio, Evan Cull, Ronald Stack and Remy Tumbar for comments and assistance with this project. This work was supported by the Defense Advanced Research Projects Agency through Army Research Office grant DAAG55-98-1-0039.